Faculty and Researchers   Faculty and Researchers' Publications

2015-10

Lagrangian vortices in developing tropical cyclones

Rutherford, B.; Dunkerton, T.J.; Montgomery, M.T.

Royal Meteorological Society

RMetS

Royal Meteorological Society

Lagrangian vortices in developing tropical cyclones

B. Rutherford,[a]* T. J. Dunkerton[a] and M. T. Montgomery[b]

[a]*Northwest Research Associates, Redmond, WA, USA*
[b]*Naval Postgraduate School, Monterey, CA, USA*

*Correspondence to: B. Rutherford, NorthWest Research Associates, PO Box 3027 Bellevue, WA 98009-3027, USA.
E-mail: blake5rut@gmail.com*
This article has been contributed to by a US Government employee and his work is in the public domain in the USA.

Tracking pre-genesis tropical cyclones is important for earlier detection of developing systems as well as targeting potential locations for dropsondes in field experiments. The use of a reference frame moving with the disturbance gives a more accurate depiction of streamlines and closed circulation than the Earth-relative frame. However, identification of recirculating regions does not require a choice of reference frame when marked by the Galilean invariant Eulerian Okubo–Weiss (OW) parameter. While the Eulerian OW parameter is generally effective at identifying vortex cores at a given place and a given time, it has its limitations in weak disturbances and in time-dependent flows. Integrating the eigenvalue of the velocity gradient tensor along particle trajectories provides a time-smoothing of the Eulerian OW parameter, and provides earlier detection with fewer false alarms. We refer to this integration along trajectories as the Lagrangian OW parameter. When mapped to a horizontal grid it becomes a Lagrangian OW field.

The Lagrangian OW field has advantages over the Eulerian OW field in the detail of additional flow structures that it identifies. The Lagrangian OW field shows the Lagrangian boundaries that are present as a disturbance develops from an easterly wave, and a shear sheath that forms when a disturbance becomes self-sustaining, typically at tropical storm strength. Since all of these structures are Lagrangian, they are advected with the flow field, and display the continuous evolution of coherent flow features as the fluid evolves.

Examples of the use of the Lagrangian OW field are given for ECMWF forecast data from the 2014 Atlantic hurricane season. All of the Lagrangian coherent structures that can be identified by this field are shown for developing disturbances and mature cyclones. The Lagrangian OW field also shows additional details of vortex mergers, and is used to identify a stable crystal lattice configuration in which vorticity does not aggregate.

Key Words: vortex identification; Lagrangian coherent structures; tropical cyclogenesis

Received 1 March 2015; Revised 15 June 2015; Accepted 25 June 2015; Published online in Wiley Online Library

1. Introduction

The question of development versus non-development of tropical disturbances has been studied extensively in both numerical studies and in recent field experiments (Pre-Depression Investigation of Cloud systems in the Tropics (PREDICT) and NASA-Hurricane Severe Storm Sentinel (HS3)). The results of these experiments have revealed many things about the dynamics of tropical cyclone genesis, and have led to new numerical techniques for evaluating pre-genesis disturbances for their potential for genesis.* The overarching framework for tropical cyclogenesis is the marsupial paradigm (Dunkerton *et al.*, 2009), where a wave-relative reference frame may be used to detect recirculation before it can be seen in the Earth-relative frame, and to diagnose the robustness of the wave's 'pouch' that protects the developing vortex. Cyclogenesis typically occurs near the intersection of the wave's trough axis and critical layer. In the wave-relative frame, a 'cat's eye' forms in the co-moving streamline field at the exterior of the disturbance, providing some protection until vorticity aggregation and amplification through convection and vortex stretching forms a dynamically protected vortex that can be sustained by sea-surface fluxes. A saddle or pair of saddles have translating streamlines that form

---

*These techniques have been used in the 'pouch products' by the Montgomery research group at Naval Postgraduate School as a way to locate pre-depression disturbances and to increase forecast lead times, and are an important tool for use in field experiments.. The pouch products

as well as the Lagrangian OW field introduced here can be seen at http://www.met.nps.edu/∼mtmontgo/storms2014.html; accessed 21 July 2015.

the cat's eye boundary and protect the nascent vortex from its environment. The existence of a cat's eye boundary is a necessary but not sufficient precursor to cyclogenesis, as many studies have concluded that a permeable pouch may inhibit genesis (Rutherford and Montgomery, 2012; Davis and Ahiyevich, 2012; Smith and Montgomery, 2012). For genesis to actually occur, the pouch must also be in a thermodynamically favourable environment, where there is a continued supply of fuel and limited 'antifuel' that could be supplied, e.g. by excessive vertical wind shear (much larger than $\sim 12\,\mathrm{m\,s}^{-1}$ in the deep troposphere; Dunkerton *et al.*, 2009). In this article, we introduce a technique using the integration of Lagrangian trajectories which improves on the translating Eulerian frame by objectively identifying pre-genesis disturbances and their boundaries, allowing the permeability of the pouch and the transition from a pouch to a self-sustaining vortex to be seen more clearly.

Amplification and aggregation of vorticity typically occurs at a smaller spatial scale within the cat's eye. The scale of the solid-body core where vorticity is maximal is also much smaller, typically less than 100 km radius, while the cat's eye boundary may be several hundred km radius. While the outer cat's eye boundary forms in the pre-depression stage, organization of vorticity into a single vortex core with little deformation typically occurs later (Montgomery *et al.*, 2010), at the tropical depression or tropical storm stage. Until now, identifying the outer boundary and inner core features has required separate techniques.

Translating streamlines in the wave-relative frame mark the cat's eye outer boundary and the horizontal gradient of translating stream function measures rotational flow velocity, but these conventional metrics do not readily identify where deformational vorticity gives way to rotational vorticity approaching centre. Strain-free rotation as measured by the Eulerian Okubo−Weiss (OW) parameter can be used to measure the strength of a vortex and its tendency toward solid-body rotation. Large values of OW parameter indicate a protected vortex whose vorticity has aggregated into a self-sustaining entity. The OW parameter is Galilean invariant, i.e. independent of the Eulerian reference frame. As the vortex becomes self-sustaining, a boundary of high differential rotation at the exterior of the solid-body core forms, serving to isolate the core from the outer flow. This shear sheath is an additional barrier which further protects the core from horizontal intrusions of dry air or low vorticity, but is not easily identified in the Eulerian OW field.

In summary, a developing disturbance requires a robust pouch boundary, an isolated vortex core of solid-body rotation, and a thermodynamically favourable environment leading to the up-scale enhancement of the system-scale vorticity. These features are currently identified separately. The boundary is identified by computing the manifolds as translating streamlines emanating from saddle points in the wave-relative frame, while the vortex core is identified as a maximum of the OW parameter. There are two improvements on the current methods that we seek to make in this study. First, we look for a diagnostic that is applicable on the spatial scales of both the pouch boundary and the inner core so that the boundary and core can be identified simultaneously. Second, since the Eulerian OW and Eulerian cat's eye boundaries both suffer inaccuracies due to the time-dependence of the flow, and the latter is frame-dependent, we formulate a new metric that is applicable to time-evolving flows and is independent of the choice of Eulerian reference frame.

The translating Eulerian cat's eye boundary is only an approximation to the Lagrangian flow, and may be permeable to Lagrangian transport even when the boundary is apparently closed in the Eulerian frame. There are two facets to this problem: (i) the degree of pouch closure at a given time and place requires consideration of recent nearby isotachs or stream function gradient, and
(ii) even if the closure is expected to become nearly complete, small fluctuations of background flow create large deviations of material contours approaching a hyperbolic point.

The outer boundaries in the time-dependent flow can be seen by stable and unstable manifolds of hyperbolic trajectories (Lussier *et al.*, 2015) or by their representation as Lagrangian coherent structures (LCSs; Rutherford and Montgomery, 2012), and in some cases differs drastically from the translating Eulerian boundaries.

While manifolds and other regions of strain are typically represented poorly by the Eulerian OW parameter, vortex cores are better represented (Basdevant and Philipovitch, 1994). Improvements to the OW criterion and Lagrangian versions of it have been used for Lagrangian vortex identification (Hua and Klein, 1998; Lapeyre *et al.*, 1999; Klein *et al.*, 2000; Haller, 2005; Lukovich and Shepherd, 2005; Haller and Beron-Vera, 2013). Though vortices are more persistent through time-dependent flows than hyperbolic lines, their identification can still be difficult with the Eulerian OW parameter in relatively weak vortices, as in developing disturbances that have not yet attained tropical storm strength. The Eulerian OW field seen in global forecast model data is typically very noisy, and it is difficult to identify and track vortices on the basis of this field alone. Lagrangian methods to identify vortices can improve their detection and tracking in time-dependent flows and locate only the more persistent vortices.

In this article, we show how a Lagrangian OW criterion can be used to identify Lagrangian vortices and their boundaries for developing disturbances in a single scalar field. We take an approach similar to other LCS identification methods by constructing a scalar field from quantities integrated along particle trajectories. Specifically, we integrate the square root of the Eulerian OW value, and we then add integrated along particle trajectories, and we then add conditional terms to this definition. This field has additional advantages over the Eulerian fields. First, it shows the Lagrangian boundaries and vortex cores which are a more accurate representation of the movement of air masses and are advected by the flow field. Second, this field shows a shear sheath at the exterior of a vortex core once it has become dynamically protected. This field also shows details of vortex merger that cannot be seen in Eulerian fields as well as some interesting configurations of small vortices that are resistant to merger. The Lagrangian OW field is a time-smoothing operation that reduces the noise of short-lived vortices, and is thus effective at identifying potential developing disturbances earlier. Our diagnostic is particularly suited for applications to weather forecasting, and for differentiating the relative strengths of vortices.[†]

An overview of other Eulerian and Lagrangian diagnostics and a definition of the Lagrangian OW field are given in the next section. Applications of this method for identifying flow features in global forecast model data are given in section 3 and are followed by a discussion of potential applications.

2. Methodology for Lagrangian vortex identification

Before introducing our Lagrangian OW diagnostic for boundary and vortex core identification, we first give a more precise definition of these flow features. The wave pouch that guides a tropical disturbance, and provides some protection for it, is composed of an outer boundary, often in a cat's eye configuration, and an inner region of recirculation. To define the outer pouch boundary, we assume for now that velocities are viewed in the translating Eulerian frame co-moving with the disturbance. Stagnation points $\mathbf{x}_{\mathrm{sp}}$ are points where fluid velocities vanish in the translating frame, $\mathbf{u}\{\mathbf{x}_{\mathrm{sp}}(\mathbf{t}),t\} = 0$ where $\mathbf{u}(\mathbf{x}(t),t)$ are the fluid velocities at the location of a trajectory $\mathbf{x}(t)$ at time t. A stagnation point is hyperbolic, or a saddle, if $\nabla\mathbf{u}(\mathbf{x}_{\mathrm{sp}})$ has real eigenvalues of opposite signs, indicating both expansion and contraction of an air parcel centred at $\mathbf{x}_{\mathrm{sp}}$. The eigenvectors of the eigenvalues

---

[†]When applied in near-real time, our method spans a time interval including prior analyses and short-term (84 h) forecast data.
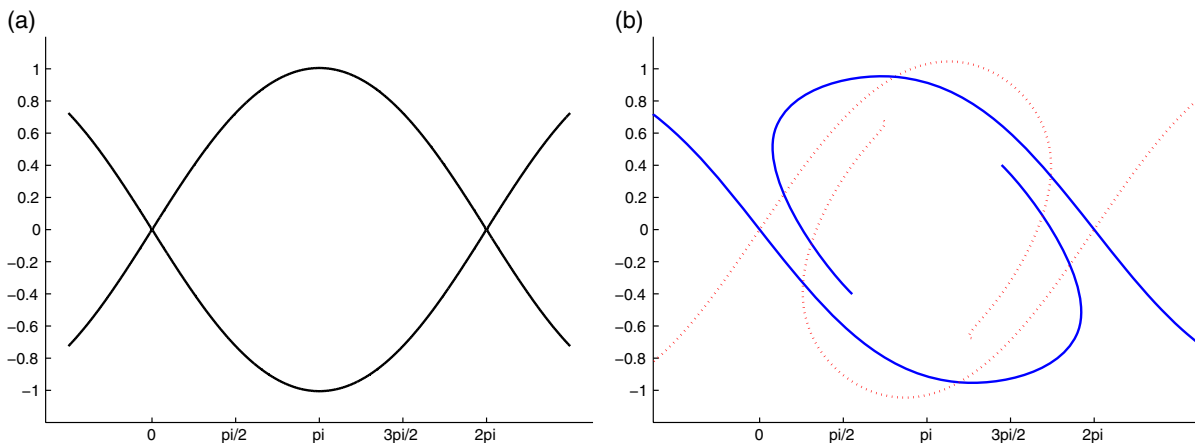
Figure 1. (a) The Eulerian manifolds of a cat's eye and (b) the Lagrangian manifolds resulting from a periodic perturbation of velocities, with stable manifolds in red (dotted) and unstable manifolds in blue (solid).

of $\nabla \mathbf{u}$ show the directions of greatest contraction/expansion along the eigenvector of the negative/positive eigenvalue. The stable/unstable manifolds for fixed t are defined as the translating streamlines[‡] that pass through the stagnation point in the direction of the eigenvector associated with the negative/positive eigenvalue. In steady flows, streamlines are transport barriers, so the stable and unstable manifolds of the saddles form the cat's eye boundary that differentiates the outer flow from the recirculating inner flow.

2.1. Stable and unstable manifolds of a hyperbolic trajectory and lobe dynamics

In time-dependent flows, these Eulerian manifolds are no longer barriers to transport, and the pouch may in fact import air from, or exchange air with, its environment. Lagrangian manifolds are related to their Eulerian counterparts, but describe more accurately the interaction of the pouch with its environment as they are material curves which are advected with the flow field. For a velocity field with time-dependence, saddle points may serve as markers for a hyperbolic trajectory (Ide *et al.*, 2002). A hyperbolic trajectory is a trajectory $\mathbf{x}_h(t)$ such that the linearized system for a perturbation $\boldsymbol{\xi}(t)$ to a trajectory

$$\dot{\boldsymbol{\xi}} = \nabla \mathbf{u}(\mathbf{x}(t), t)\boldsymbol{\xi} + \mathcal{O}(|\boldsymbol{\xi}^2|) \qquad (1)$$

has linearly independent solutions which exhibit exponential growth and decay. The stable and unstable manifolds of the hyperbolic trajectory form flow boundaries in time-dependent flows. A boundary comprised of both stable and unstable manifold segments that forms a flow partition is called a separatrix, and may differentiate physically important regions. If the flow were steady in some frame of reference, the separatrix would remain fixed and would mark an actual flow boundary. However, in a time-dependent flow, the Eulerian separatrix may be semipermeable owing to the intrinsic time-dependence in the co-moving frame. As the flow evolves with time, the separatrix must be redefined so that it is most similar to what is expected from the Eulerian flow (Rom-Kedar *et al.*, 1990). Enclosed regions called lobes may form from segments of Lagrangian manifolds which intersect at locations other than at the hyperbolic trajectory. Rearrangement of lobes allows the contents of the lobe to be transported across the Eulerian boundary as the separatrix is redefined. Lobe dynamics

describe transport due to the movement of lobes, e.g. a perturbed Kelvin–Stuart cat's eye flow (Rodrigue and Eschenazi, 2010).

The effect of time dependence on the cat's eye boundary can be demonstrated by a schematic of the basic structure of the cat's eye in Figure 1. In (a), the Eulerian cat's eye is shown where the stable and unstable manifolds of a saddle point coincide to form a barrier. In time-dependent flows, illustrated by time-periodic forcing applied to the cat's eye flow (b), the manifold structure is more complicated, and transport through lobes allows transport across the Eulerian boundary, but the amount of material transported is limited to what is contained in the lobes. The stable manifolds (red) intersect the unstable manifolds (blue) in multiple locations, and enclosed lobes interior and exterior to the Eulerian cat's eye (shown in black) are transported across the boundary. Including divergence introduces an additional pathway of entrainment through non-intersecting manifolds which allow an open pathway of material to enter in (Riemer and Montgomery, 2011). Lussier *et al.* (2015) gives examples of how these manifold boundaries can be used to identify the boundaries in pre-genesis disturbances.

Computing hyperbolic trajectories and their manifolds requires first the location of persistent stagnation points, which requires an appropriate frame of reference and may be very sensitive to the choice of reference frame or data errors. Finite-time Lagrangian methods avoid this difficulty by locating the manifolds directly. Repelling and attracting LCSs are maximal ridges of the forward- and backward-time Lagrangian fields, and play the role of stable and unstable manifolds over the finite integration time (Haller, 2000; Shadden *et al.*, 2007). There are many methods for locating LCSs using Lagrangian scalar fields.[§] The idea behind these methods is that particles which are initialized on opposite sides of a manifold experience the greatest relative separation, thus the manifold is a maximum of a scalar field measuring relative separation. Similarly, trajectories which have the highest average strain rates should lie on manifolds, and this idea will be important in the construction of the Lagrangian OW field.

These Lagrangian manifolds have been used to show that dry air entering a pouch lacking a fully developed unstable manifold on one side may be detrimental to genesis (Rutherford and Montgomery, 2012), while interactions limited by the lobe dynamics mechanism may still allow genesis (in progress). Interaction with the outer environment may even help genesis, as in the case of hurricane *Sandy* where moist air with high vorticity was imported through a large pouch opening to the south (Lussier *et al.*, 2015).

[‡]The Eulerian manifolds, the stable and unstable manifolds of a hyperbolic fixed point or saddle, and streamlines emanating from a saddle all refer to the same Eulerian flow structure. A key point is that the identity of a stagnation point is frame-dependent. The velocity gradient tensor and its eigenvalues (eigenvectors) are Galilean invariant, but the choice of a particular pair of eigenvectors as belonging, e.g., to a hyperbolic point is frame-dependent.

[§]Among these methods are finite-time Lyapunov exponents (FTLEs), finite-size Lyapunov exponents (FSLEs), Lagrangian descriptors, and strain lines. We refer the reader to Haller (2015) for a summary of these methods.
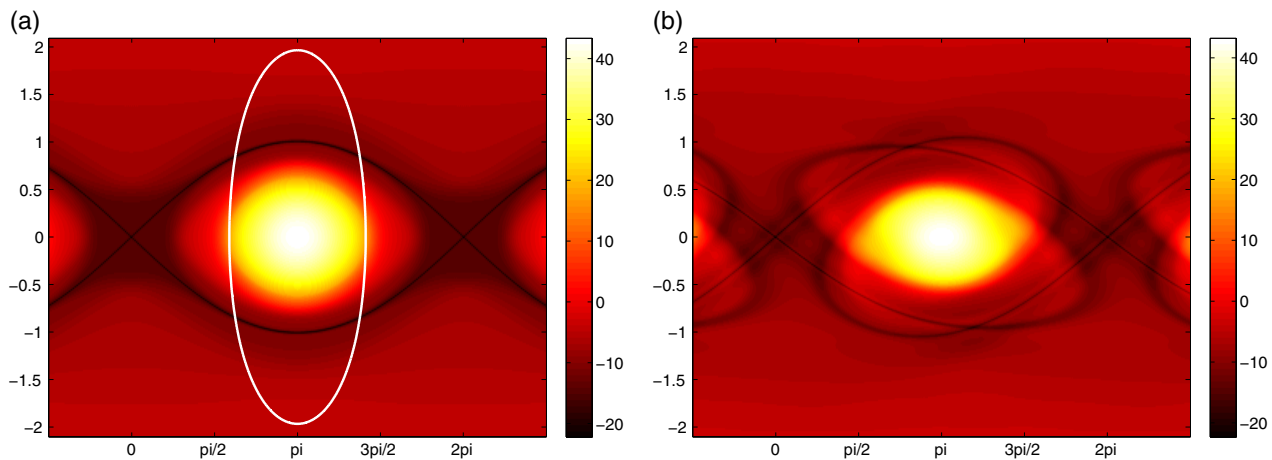
Figure 2. The OW_{Lag} fields are shown for the Kelvin–Stuart cat's eye (a) for a steady flow with the $OW = 0$ contour (white) overlaid, and (b) with time-dependence. In both the steady and unsteady cases, the manifolds can be seen at the edge of the cat's eye as the lines with the most negative values, and the vortex core can be seen as the circular region with the most positive values.

2.2. Vortex core identification

In steady flows, vortex core identification is typically separate from identification of the kinematic boundary induced from the large-scale flow. However, the two identification problems are not unrelated since elliptic stagnation points (also called centres or nodes), emerge in a one-to-one ratio with saddles in a saddle-node bifurcation. Similar to hyperbolic stability, elliptic stability is determined the eigenvalues of $\nabla \mathbf{u}(\mathbf{x})$. Since a two-dimensional vortex core is in near-solid-body rotation, the entire vortex core has elliptic stability.

The OW (Okubo, 1970) criterion partitions the flow into rotation- and strain-dominated regions based on the stability of particles. Assume that the flow is non-divergent, $\delta = u_x + v_y = 0$, and again, let $\mathbf{x}$ be the location of a particle and $\boldsymbol{\xi}(t)$ a perturbation to the particles' position. Stability of $\boldsymbol{\xi}(t)$ is determined by behaviour of the exponential solutions to Eq. (1), given by

$$\boldsymbol{\xi}(t) = \exp\left(\lambda_{\pm} t\right) \boldsymbol{\xi}_0. \tag{2}$$

The eigenvalues of $\nabla \mathbf{u}$ are $\lambda_{\pm} = \pm\sqrt{-OW}$ and

$$OW = \frac{1}{4}\left(\zeta^2 - s_1^2 - s_2^2\right), \tag{3}$$

where $s_1 = u_x - v_y$ and $s_2 = v_x + u_y$. The eigenvalues of $\nabla \mathbf{u}$ are imaginary and $\boldsymbol{\xi}(t)$ is a rotation about $\boldsymbol{\xi}_0$ when $OW > 0$. Solid-body rotation occurs when $s = s_1^2 + s_2^2 = 0$ and elliptic rotation occurs when $|\zeta| \geq |s| > 0$. If $OW < 0$, the eigenvalues are real and $\boldsymbol{\xi}(t)$ grows exponentially in the direction of the eigenvector corresponding to the positive eigenvalue. Improvements to the OW criterion include adding divergence (Lukovich and Shepherd, 2005) and additional terms in the Taylor expansion of the perturbation[¶] (Hua and Klein, 1998; Lapeyre *et al.*, 1999).

2.3. Lagrangian vortices

The OW criterion determines elliptic stability where the growth of the perturbation $\boldsymbol{\xi}(t)$ is small, and thus the linear approximation of $\boldsymbol{\xi}(t)$ remains valid. This condition is generally valid for long periods of time only in vortex cores where the velocity gradient varies slowly relative to the vorticity gradient (Basdevant and Philipovitch, 1994). Once the time dependence of velocities

following an air parcel is sufficiently large that the perturbation cannot be well approximated by the linear approximation, OW ceases to be a meaningful quantity. Motivation for a Lagrangian OW criterion in the case of cat's eyes with small wave amplitude can be seen in Figure 2(a), where the region of recirculation according to the OW criterion, the interior of the white circle, lies partially outside the cat's eye boundary.[‖] In this example, the flow is steady so the manifolds are a complete barrier to transport and are seen as dark red curves. Haller and Poje (1997) have noted that trajectories that remain in vortex cores satisfy the OW condition for elliptic stability for longer times than generic trajectories, and define a Lagrangian OW criterion based on the time that trajectories spend in elliptic or hyperbolic regions.

Other methods of objectively identifying vortices are shown in Haller (2005) and Beron-Vera *et al.* (2010). The scalar field formed by the time integral of OW values, or of other invariants of the velocity gradient tensor, locates hyperbolic manifolds at locations where the field attains a minimum value in our sign convention (Pérez-Muñuzuri and Huhn, 2013). The variational Lagrangian coherent structure methods of Haller (2011) and Farazmand and Haller (2012) are also capable of detecting hyperbolic, elliptic, and shearing structures, but require an additional computation to find the streamlines of the vector field formed from the eigenvector associated with the eigenvalue of minimum modulus of the Cauchy–Green deformation tensor. The Lagrangian boundaries may be further distinguished as those that are locally least-stretching (Haller and Beron-Vera, 2012). These variational methods are purely kinematic, i.e. they do not account for the magnitude or distribution of vorticity in distinguishing important flow regions. Instead, they have the primary objective of identifying vortex boundaries. The methods developed here are designed specifically to identify the regions of strongest and continuous rotation in flows with strong vorticity gradients.

2.4. Lagrangian OW

The Lagrangian OW formulation that we give is intended to address some concerns which we have with the other Eulerian and Lagrangian diagnostics we have referred to, including:

1. The pouch boundary and vortex core must be diagnosed separately;

[¶] In the examples shown, our trajectories are driven by the full (rotational plus divergent) flow, but the contribution of divergence to the eigenvalue is ignored, being negligible in the lower free troposphere. Horizontal divergence δ adds a term $\delta/2$ to the eigenvalue, and a term δ^2 inside the parentheses of OW.

[‖] In this example, we use the Kelvin–Stuart cat's eye defined by the streamfunction $\psi(x, y) = -\log(a \cosh y + \sqrt{a^2 - 1} \cos x)$. We find that for values of $a < 1.16$, the OW criterion fails for a portion of trajectories.

2. Time-dependence may make Eulerian manifolds permeable to transport, hence the question of whether the pouch is closed or open cannot be answered using Eulerian velocity data;

3. OW does not accurately diagnose vortex cores in thin cat's eyes;

4. OW is a noisy field due to the convectively instability of the tropical atmosphere in pouches (Smith and Montgomery, 2012), and thus the persistent injection of related small-scale features in the ordinary OW field, which makes it difficult to isolate independent, long-lasting vortices in pre-genesis flows.

5. Lagrangian vortices are identified as impermeable elliptic regions, but the Lagrangian scalar field methods do not distinguish vortex strength.

Many methods of locating Lagrangian vortices measure the time particles spend rotating but do not include the strength of the rotation, which can be seen in the Eulerian OW field. By including the strength of vorticity, a quantity can be computed that differentiates quickly rotating regions such as hurricane-like vortex cores from other slowly evolving rotational regions. For cyclogenesis, this is an important addition since the strength of vorticity relative to strain is suggested to be an important factor for cyclogenesis to occur (Tory *et al.*, 2012). We call the eigenvalue λ_+ of $\nabla \mathbf{u}$ the effective rotation rate of a particle since an air parcel subject to strain will be deformed and have a slower rotation rate (Roulstone *et al.*, 2015). This quantity has the same units as vorticity. By integrating the effective rotation rate along air parcels, we define the accumulated number of effective rotations as

$$F(x(t)) = \int_I \lambda_+(\mathbf{x}(t)) \mathrm{d}t, \tag{4}$$

where I is an interval of time chosen where velocity information is available. We note that the field F is complex valued, with real numbers marking deformation dominated regions and imaginary numbers marking vorticity dominated regions. The field defined by $\mathrm{imag}(F) - \mathrm{real}(F)$ shows vortices as maxima and manifolds as minima and would be considered the more general Lagrangian OW field. For this study, we are more concerned with cyclonic vortices, which leads to the definition of the quantity

$$G(\mathbf{x}(t)) = \int_I \lambda_+(\mathbf{x}(t)) S(\mathbf{x}(t)) \, \mathrm{d}t, \tag{5}$$

where the function S is defined as

$$S = \begin{Bmatrix} \mathrm{sgn}(\zeta); & \lambda \ \mathrm{imag} \\ 1; & \lambda \ \mathrm{real} \end{Bmatrix} \tag{6}$$

and differentiates cyclonic and anticyclonic vortices. We are most interested in the extreme values of each of these fields, and we define the Lagrangian OW field as

$$OW_{\mathrm{Lag}} = \mathrm{imag}(G) - \mathrm{real}(G). \tag{7}$$

The OW_{Lag} field can be thought of as the number of effective rotations of an air parcel, with values of 2π marking one full rotation. Since the quantities being integrated do not depend on the choice of inertial coordinate frame, OW_{Lag} is a Galilean invariant quantity. Large negative values of OW_{Lag} mark shearing or hyperbolic regions while positive values mark cyclonic vortex cores. Though manifolds, shear sheaths, and anticyclonic vortices all appear as negative values, there is little ambiguity in differentiating these features due to the differences in their shape and their relation to cyclonic vortex cores. The difference between the shear sheaths and cat's eye boundaries can be determined by the shape of the boundary and proximity to the vortex core, since shear sheaths reside just exterior to the vortex core. Anticyclonic vortex cores are circular regions with no positive maximal value. The OW_{Lag} field allows manifolds, shear lines, and vortex cores all to be identified in a single field, with stronger vortices the most prominent.

OW_{Lag} is shown for the steady Kelvin–Stuart cat's eye in Figure 2(a) and for the same flow with a periodic time perturbation in (b). In the steady flow, OW_{Lag} eliminates the curvature problem present in the OW field, as the OW_{Lag} positive values are contained within the cat's eye boundary.

In Figure 2(a), the flow is steady so the stable and unstable manifolds coincide. In Figure 2(b), a periodic time-dependent term has been added to the streamfunction which leaves hyperbolic trajectories, but alters the shape of the manifolds, seen as curves with the lowest OW_{Lag} values. The stable and unstable manifolds seen in the OW_{Lag} field do not coincide, and thus allow for the transport of fluid between the vortices. The same lobes that were visible from direct computation, Figure 1(b), are visible in the OW_{Lag} field, Figure 2(b). For longer integration times where manifold segments accumulate near the hyperbolic trajectory, lobe dynamics are revealed in the OW_{Lag} field by 'thick' manifolds, where multiple manifold segments are in close proximity to each other. Lobe dynamics is a non-divergent process where the amount of material transported into the pouch is limited to what is contained in the lobes. On the other hand, open pathways to transport are seen where manifolds of short length do not reach another hyperbolic trajectory, and may be caused by convergent flows or larger time-dependence. In the flows studied here, the finite-time manifolds cannot capture the lobe transport mechanism since they are non-intersecting. The open pathway to transport is a fast process where the amount of environmental air that can directly impact the core is potentially unlimited.

The time interval I is the interval over which particle trajectories are integrated. For most Lagrangian scalar field methods, a forward integration reveals stable manifolds (repelling LCSs) while a backward integration reveals attracting LCSs (unstable manifolds). Our cat's eye boundary is composed of a combination of stable and unstable manifolds so we let I straddle the time interval of the initial time of trajectory integration. The difference between the stable and unstable manifolds is not shown in this field, but can be inferred by looking at the geometry of the cat's eye where the unstable manifolds emanate from hyperbolic trajectories on the northeast and southwest boundaries of the pouch and the stable manifolds on the northwest and southeast boundaries. The length of the time interval is chosen to be characteristic of the flow. For the flows observed during cyclogenesis, the time required for air parcels to travel from near one hyperbolic trajectory to near the other is on the order of 1 day, so a choice of integration time must be longer than 24 h in each direction in time to resolve the manifolds effectively.

While the exact mechanism of entrainment into the pouch is an interesting problem, it requires the complete computation of stable and unstable manifolds and cannot be answered by this method. However, the question which is of primary concern in forecasting is the influence of environmental air on the pouch; does the environmental air enter in? The OW_{Lag} field addresses this question by showing the width of the region of ingestion (Figure 3(a)). In the case of an open pathway, no manifold will be present at the pouch opening. In the case of lobe dynamics, the manifold is blurred by the fact that air parcels contained in lobes mix into the pouch where they spend time in vorticity-dominated regions. In either case, a manifold which terminates before reaching the second hyperbolic trajectory indicates that the pouch has an opening to transport of environmental air.

All of the flow features that are present in the steady and periodically perturbed flows can also be identified in global forecast model data. An example of this field for ECMWF forecast data at 1800 UTC 14 September is shown in Figure 3(b). To produce the fields shown in these examples, a grid of trajectories in integrated both forward and backward for 36 h from the initial location, and OW_{Lag} is evaluated along the trajectories by Eq. (5),
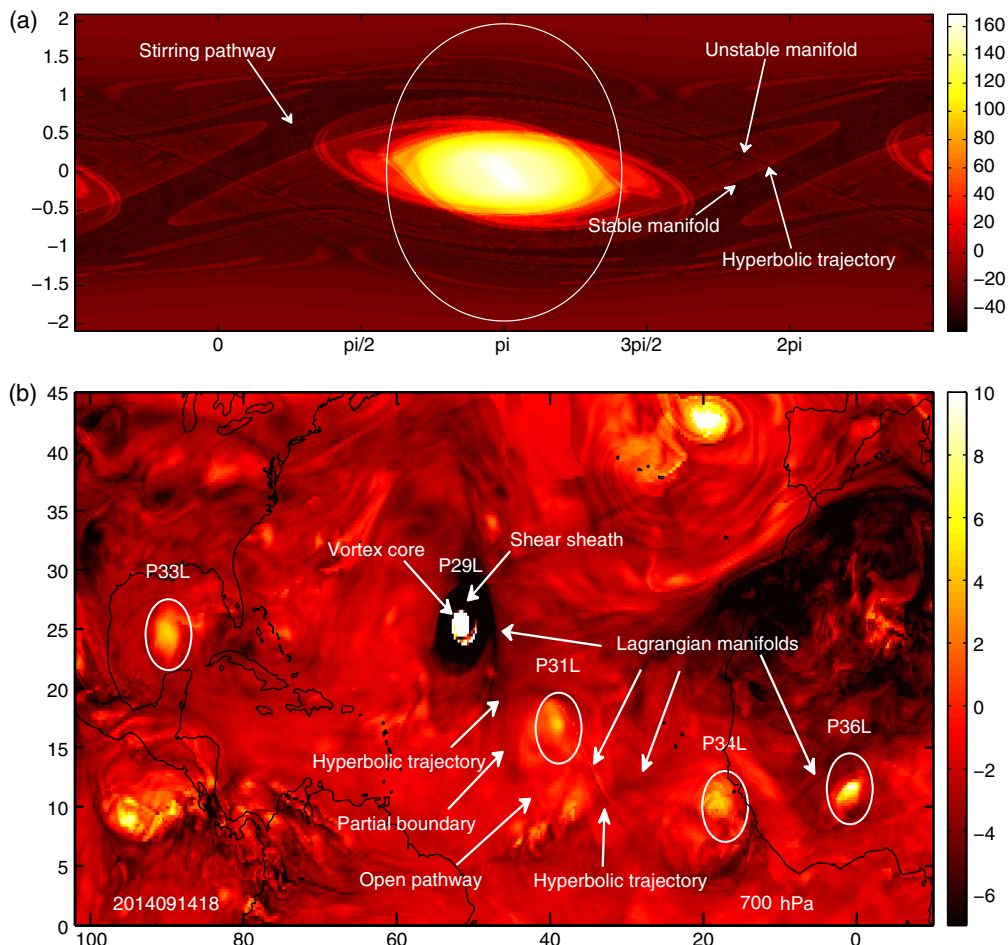
Figure 3. The OW_{Lag} field for the Kelvin–Stuart cat's eye is shown in (a) with the $OW = 0$ contour (white) overlaid. Panel (b) shows the OW_{Lag} field for the ECMWF model at 1800 UTC on 14 September 2014 at 700 hPa. Key Lagrangian flow features in both panels are labelled and indicated by arrows.

and the quantity plotted is then constructed using Eq. (7). The total length of the interval I is 72 h, and allows both the stable and unstable manifolds to be identified. The prominent flow features that we identify are:

1. Vortex cores are nearly circular regions of strain-free deformation, with particles remaining in the vortex core for long periods of time. They are seen as regions of high OW_{Lag} values.
2. Shear sheaths are circular regions exterior to the vortex core of high deformation and possess large vorticity gradients which act as barriers to transport. They can be seen in the OW_{Lag} field as large negative values just outside of vortex cores, and their presence indicates that no additional air will be interacting with the core.
3. Lagrangian manifolds are regions of high strain which form the outer pouch boundary. They can be seen as elongated regions of negative OW_{Lag} values further away from the pouch centre and typically at a distance of $3-8°$.
4. Hyperbolic trajectories are locations where two Lagrangian manifolds intersect each other. A manifold spanning between two hyperbolic trajectories forms a complete boundary, while a manifold terminating before reaching another hyperbolic trajectory indicates that transport across that region and into the pouch is occurring.

The formulation of this field is to some extent determined by what we desire to see in the given flow. Our formulation of OW_{Lag} integrates a quantity that can be positive or negative, depending on whether a trajectory is located in a hyperbolic or elliptic region. The integral of a potentially negative quantity introduces a cancellation problem. It is possible for a trajectory to

spend some time in both hyperbolic and elliptic regions, and for its OW_{Lag} value to be near 0 as the positive and negative parts in the time integral given by Eq. (5) cancel. OW_{Lag} may miss some short-lived vortices or could miss hyperbolic lines long enough to modulate stirring by lobe dynamics. These could be identified by integrating a strictly positive quantity such as the modulus of velocity (Mancho *et al.*, 2013). At the pouch boundary, the aforementioned cancellation blurs manifolds that have little role as a pouch boundary, and the length of the persistent structure gives an indication of what portion of the pouch boundary is robust. In addition, the potential cancellation actually serves to denoise the dataset and OW_{Lag} differentiates persistent vortices from transient vortical structures such as those frequently observed in the Intertropical Convergence Zone (ITCZ). When tracking in real time or developing automated methods for locating pre-genesis disturbances, this time smoothing greatly reduces the number of potential vortices that need to be examined.

3. Results

3.1. Comparison with OW

The differences between the OW and OW_{Lag} fields can be seen in Figure 4(a) and (b) respectively. The positions of different pouches are indicated by circles and are labelled in this figure and in the following figures.** The time smoothing of the OW_{Lag}

**The pouch labelling is taken from the Montgomery research group's pouch products where the number refers to the number of the pouch that is tracked for that season.
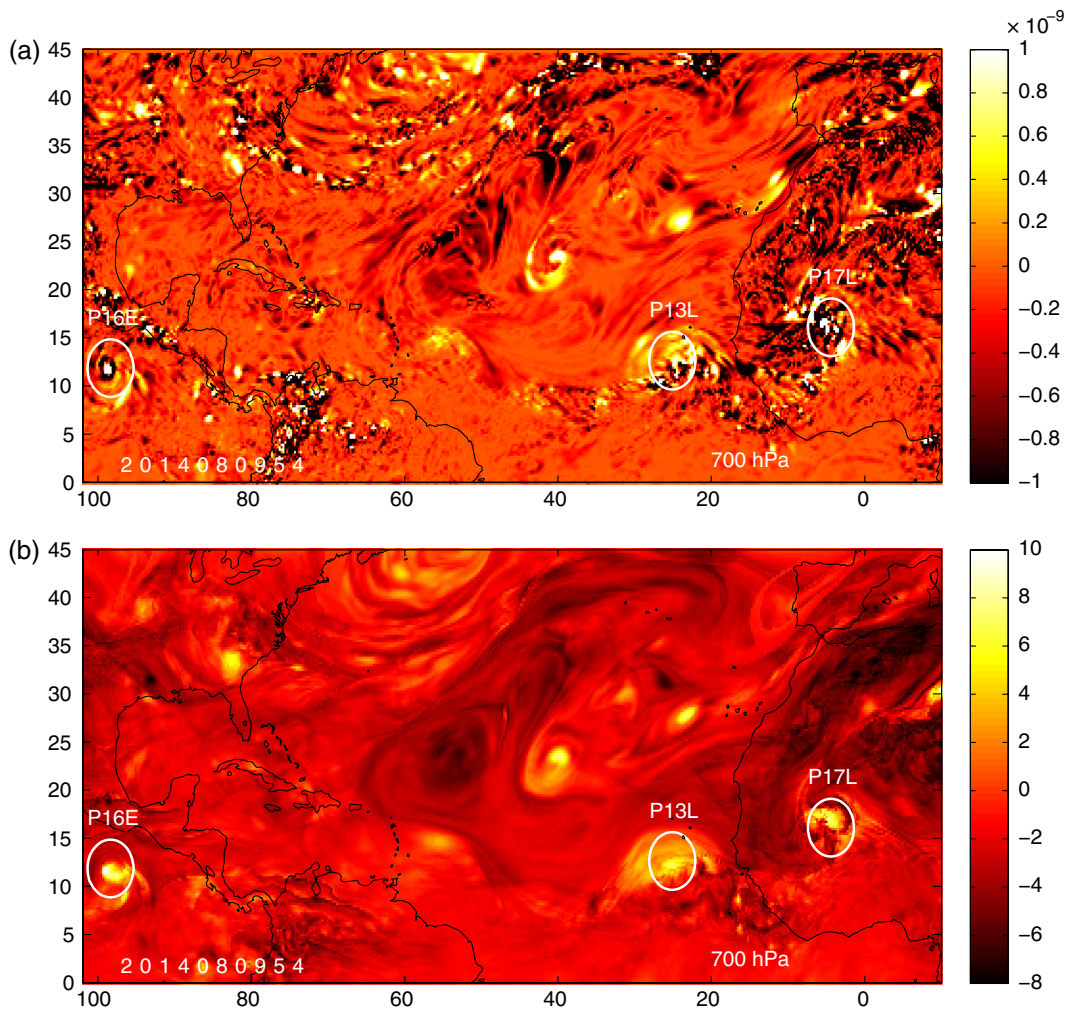
Figure 4. The (a) OW (s^{-2}) and (b) OW_{Lag} (radians) fields for the Atlantic development region at the +54 h forecast time on 9 August.

can be seen by a much smaller number of vortices. In particular, P17L is in a very noisy region in the OW field, and cannot easily be identified in this field alone. Instead, a Hövmuller of velocities is used to identify the African easterly wave and its position is then determined by the intersection of the wave's critical latitude and trough axis, a process more difficult to automate. However, OW_{Lag} clearly identifies this flow feature while ignoring the surrounding noise. While OW does not represent straining regions well, OW_{Lag} shows manifold boundaries, including the locations of cat's eyes such as those enclosing P17L and P13L and a shear sheath enclosing the core of P19L, P29L, Figure 3 (b).

3.2. Time evolution of the flow field

While strong vortices may be tracked in the Eulerian OW field, other flow features such as manifolds are in general not advected by the flow. In contrast, the OW_{Lag} field is Lagrangian in nature, which allows all flow features to be tracked. A time evolution of the flow shows a fluid-like evolution not only Figure 3(b) of vortices but also of manifolds. The time-evolution of the flow can be seen in Figure 5. The features that are identified in Figure 2(b) can be tracked for the 14 September forecast. In this field, we see a line of three cat's eyes forming the boundaries of P31L, P34L, and P36L. As these pouches move westward, the boundaries can all be identified through time evolution of the flow field. Hyperbolic trajectories located between adjacent cat's eyes can also be tracked over this time period. P31L has very weak vorticity, and its Lagrangian boundaries arise mostly P34L from the stronger flows associated with P29L (*Edouard*) and P32L.

3.3. Vortex merger and non-merger

The boundaries from the OW_{Lag} field show more details of vortex merger than can be seen in the OW field. For example, the merger of P17L and P18L on 15 August is shown in Figure 6. A well-defined separatrix separates the pouches at 1200 UTC and remains in place until +36 h. While the pouches are separated, no merger occurs. However, the boundary between the pouches changes before +66 h, and the pouches are able to merge. As the boundary changes, the hyperbolic trajectory to the east of P18L travels westward and comes in close proximity to the hyperbolic trajectory located between P17L and P18L (Figure 6(c)). At this time, there are two hyperbolic trajectories but the vorticity is mostly combined into a single entity, which was called P18L. The two hyperbolic trajectories very near each other indicate that the merger is not complete; there must also be two elliptic points remaining. The merger is complete when the hyperbolic trajectories merge and one of the centres disappears in a saddle-node bifurcation.

3.4. The shear sheath, vortex core, and manifolds of Edouard

Eduoard was one of the strongest storms of the 2014 Atlantic hurricane season and the first major hurricane since hurricane *Sandy* (2012). *Edouard* formed from a tropical wave that left Africa on 7 September, and was classified as a tropical depression on 12 September. *Edouard* was upgraded to a hurricane on 15 September. We look at the ECMWF forecast from 0000 UTC on 13 September to examine the structure of *Edouard* as it
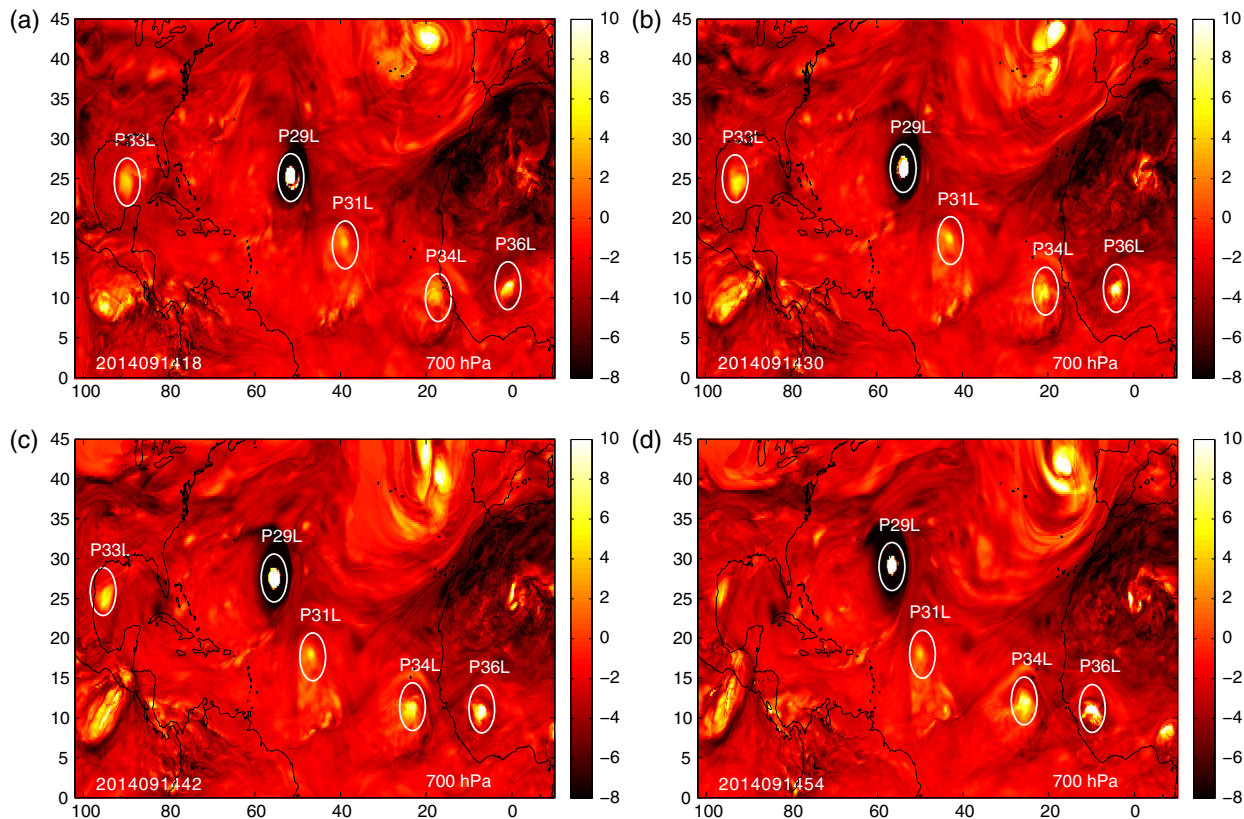
Figure 5. The time evolution of the OW_{Lag} field for the Atlantic development region on 14 September at forecast times of (a) +18 h, (b) +30 h, (c) +42 h, and (d) +54 h.
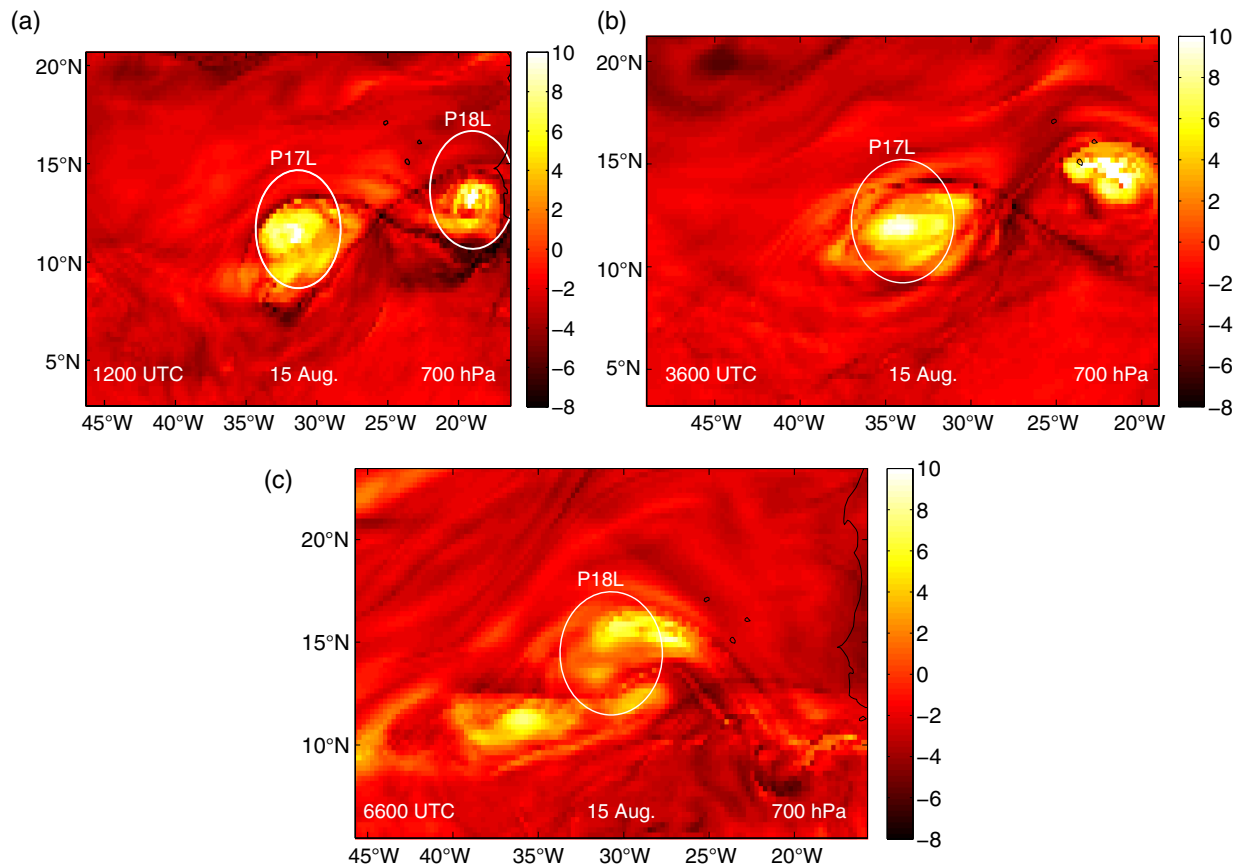

Figure 6. The OW_{Lag} fields for P17L and P18L during a vortex merger in the 0000 UTC 15 August forecast. At the forecast times of +12h (a) and +36h (b), both +36 h, both P17L and P18L are identified, but at the later time (c) +66 h the combined pouch is called P18L.
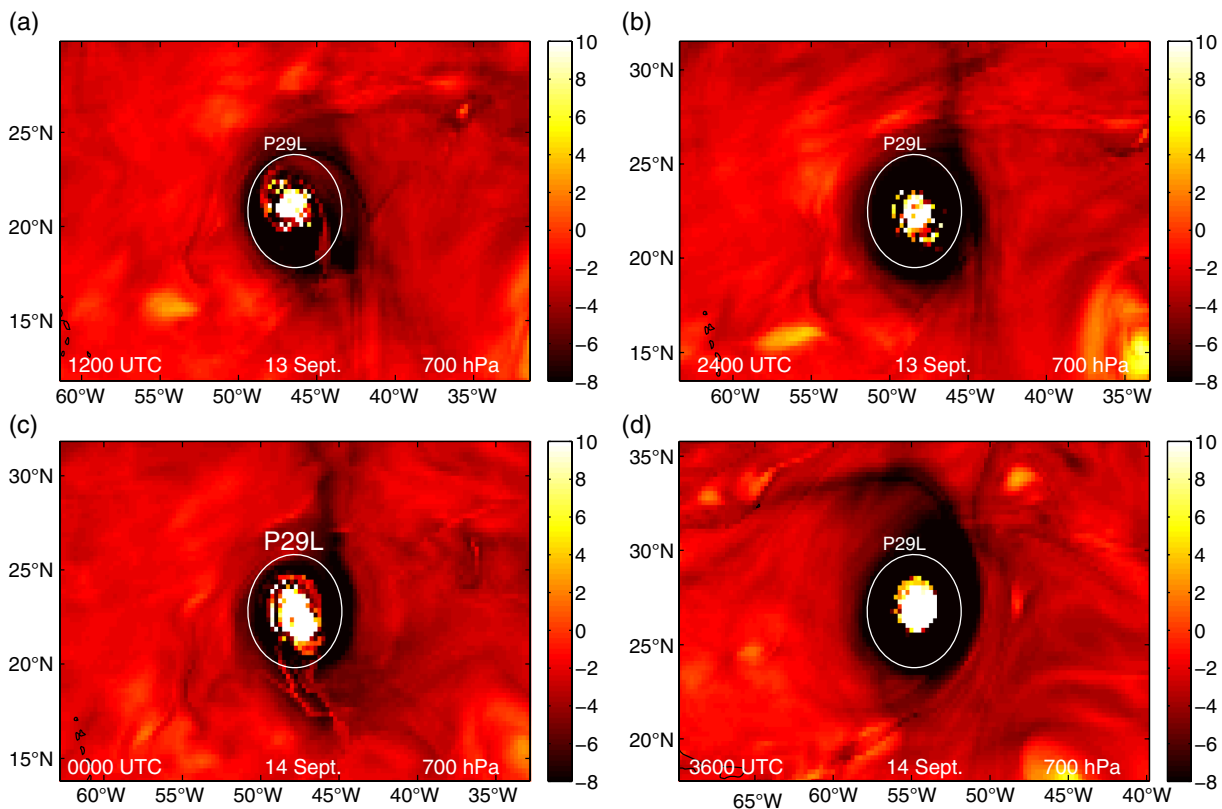
Figure 7. The 700 hPa OW_{Lag} fields for pouch P29L for analyses at (a) 1200 UTC on 13 September 2014 and (c) 0000 UTC on 14 September, and forecasts (b) +24 h from 0000 UTC on 13 September, and (d) +36 h from (c).

was transitioning from a tropical depression to a hurricane. The structure from the 700 mb OW_{Lag} field is shown in Figure 7. The transition to a shear sheath occurs near 1200 UTC on 13 September as a ring of high OW_{Lag} starts to organize around the periphery of the storm, and the shear sheath is completely formed by the 2400 UTC forecast. At 0000 UTC on 14 September the analysis data verify the forecast from the previous day, showing a well-enclosed shear sheath. Later in the forecast, the distinction between the storm and the outer flow becomes even more distinct at +36 with a large region of highly deformational flow (dark red (dark gray in print) to black). surrounding an undisturbed vortex core (white). The vortex core is comprised of nearly periodic trajectories and is not penetrated during this time interval. These closed orbits are finite-time Kolmogorov–Arnold–Moser tori, with the outermost one lying at the boundary of the vortex core and shear sheath. The vortex core is a region of minimal deformation, while the shear sheath contains the region of highest deformation where vortex Rossby waves may propagate.

3.5. Horizontal straining of P27L

While Lagrangian boundaries are required to eliminate intrusion of environmental air, and are therefore seen in most developing disturbances, the existence of Lagrangian boundaries alone does not guarantee development. This is particularly true when the boundaries do not form the typical cat's eye shape associated with cyclonic flow in the Atlantic. Environmental influences such as stronger horizontal winds at mid-levels or vertical wind shear (Riemer and Montgomery, 2011) may alter the Lagrangian boundary configuration, and thus alter the advection of vorticity. P27L was an example of a disturbance that was subjected to strong horizontal winds during the 6 September forecast. P27L has two hyperbolic trajectories with manifolds, but the hyperbolic trajectories were located to the west and north rather than the west and east. The hyperbolic trajectories and manifolds can be seen at 1800 UTC on 6 September in Figure 8(a). The angle

between the manifolds of the western hyperbolic trajectory is very large, while the length of the manifolds from the northern hyperbolic trajectory is very short. By +36 h, the northern hyperbolic trajectory vanishes (Figure 8(b)), leaving the unstable manifold from the western hyperbolic trajectory as the boundary controlling the advection of vorticity. By +60 h (Figure 8(c)), the vorticity is strained along this boundary and a coherent vortex core ceases to exist.

3.6. The multiple vortex structure of P13L

P13L had enclosed Lagrangian boundaries on the northern edge of the pouch (Figure 9), but an opening to the southern side, a typically favourable location for an opening since it would be less related to influences such as the Saharan air layer (SAL). Within the pouch, there are several pools of enhanced cyclonic vorticity which are coherent but separate. In the OW_{Lag} field, we can follow the individual vortices and see that they do not merge, though each vorticity pool retains its circulation for most of the forecast period. There are multiple reasons that the vortices do not merge. There is very little convergence, which can be seen since the area enclosed by the Lagrangian boundaries shows little change over this time period. Also, there is very little convection to assist the up-scale organization from smaller scales (Montgomery *et al.*, 2006). Since the arrangement of the vortices is in a polygonal pattern due to the triangular shape of the pouch, we note the similarity to vortex crystals seen in two-dimensional inviscid Euler flows where the configuration of vorticity acquires a state of minimum kinetic energy (Jin and Dubin, 2000). This pattern cannot be seen in the OW field.

This example shows a case where a favourable environment does not lead to genesis though the pouch boundary is closed to adverse intrusions, and confirms the necessary but not sufficient criteria of a pouch boundary. While the aggregate of these smaller structures appears to contain enough vorticity for development, there is a lack of up-scale organization toward an eyewall from
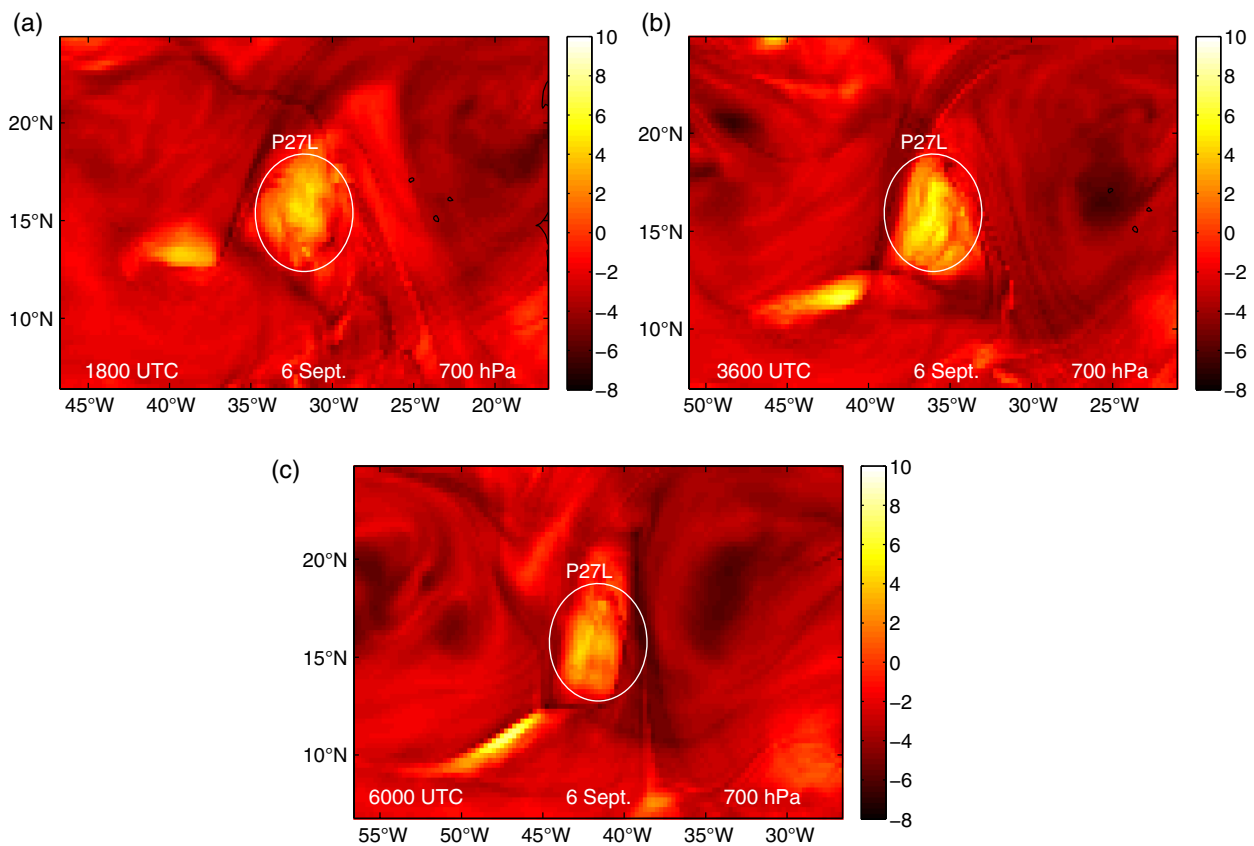
Figure 8. The 700 hPa OW_{Lag} fields for pouch P27L for the 6 September forecast at (a) +18 h, (b) +36 h and (c) +60 h.
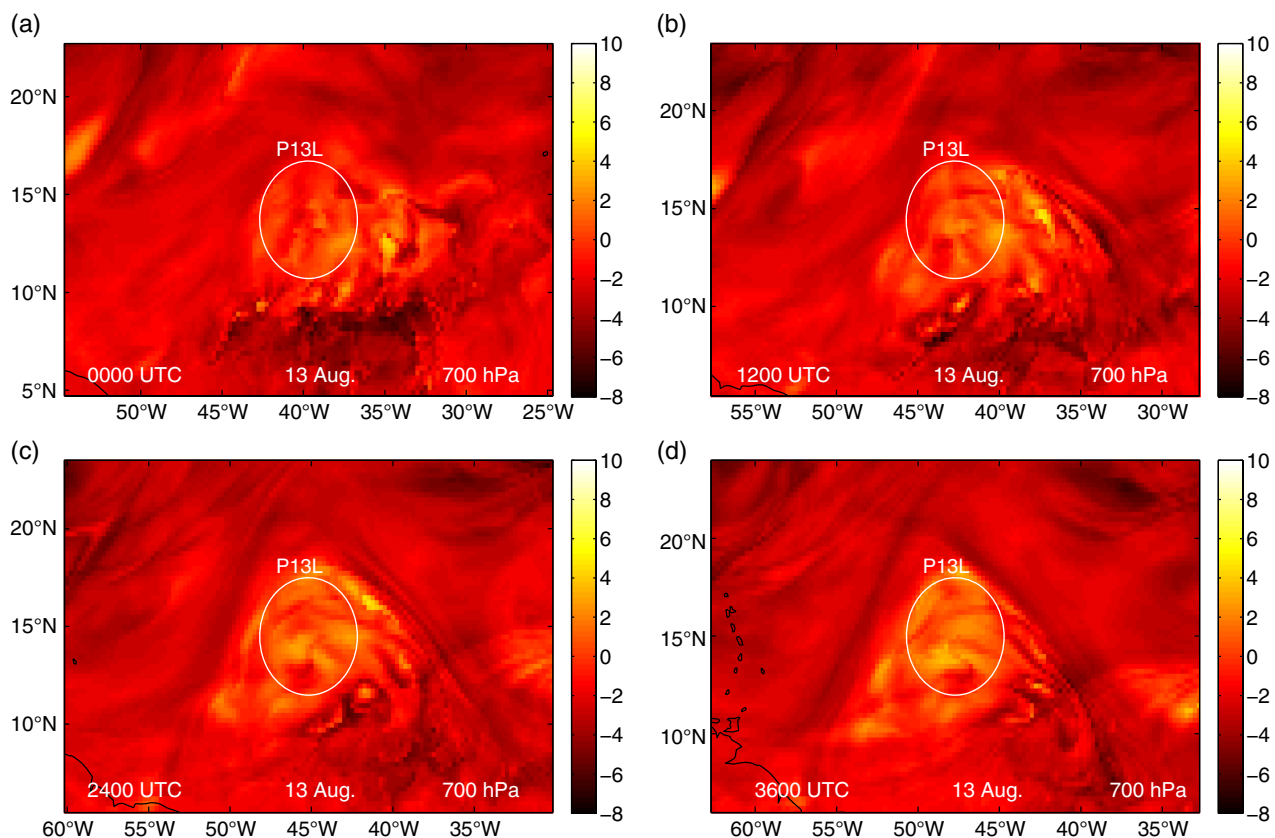

Figure 9. The 700 hPa OW_{Lag} fields for pouch P13L for the August 13 forecast at (a) 0000 UTC, (b) +12 h, (c) +24 h, and (d) +36 h. The isolated pools of moderately high OW_{Lag} within the pouch represent the non-merging pools of vorticity.

these vortices through diabatic vortex stretching or through horizontal mergers. The Lagrangian structures and their role in the merger of these smaller vorticity anomalies and diabatic activation represents an important mechanism for genesis which deserves further study. The methods used in this study are capable of resolving the features at smaller scales, but finer model resolution will be required to resolve the flow boundaries that exist between these vortices (Rutherford *et al.*, 2012).

4. Summary

We have shown that a Lagrangian OW parameter integrated along particle trajectories is a useful diagnostic for the identification of coherent vortices and flow boundaries in a time-dependent flow. The Lagrangian quantity is advected with the flow field and shows more precise boundaries than can be seen in the OW field. These additional details reveal many interesting properties of the dynamics such as vortex crystals which were not to be seen in Eulerian OW fields at the same time. Many aspects of tropical cyclogenesis can be seen in the OW_{Lag} field, including the formation and evolution of cat's eyes, vortex cores, and shear sheaths. The field also reveals the details of vortex merger, and was used to identify a crystalline vortex pattern.

The OW_{Lag} field is a time-smoothing of the velocity field, and reduces the noise seen in Eulerian fields due to transient vortices. The time-smoothing may be useful for automating the process of pouch identification and reduces the need for identification of the easterly wave since OW_{Lag} contains the time evolution of velocities that is seen in a Hövmuller plot.

While the OW_{Lag} field has the benefit of reducing false alarms by eliminating spurious vortices, we do not see a reduction of developing disturbances which are correctly identified. Since a maximum of the OW_{Lag} field appears in every tropical depression, and a shear sheath appears in every tropical storm that we have studied, these characteristics appear to be necessary conditions for storm development. The existence of a similar structure on multiple vertical levels may lead to a sufficient dynamic criterion for development.

Acknowledgements

References

Basdevant C, Philipovitch T. 1994. On the validity of the 'Weiss criterion' in two-dimensional turbulence. *Physica D* **73**: 17−30.

Beron-Vera FJ, Olascoaga MJ, Brown MG, Koçak H, Rypina II. 2010. Invariant-tori-like Lagrangian coherent structures in geophysical flows. *Chaos* **20**: 017514, doi: 10.1063/1.3271342.

Davis CA, Ahijevych DA. 2012. Mesoscale structural evolution of three tropical weather systems observed during PREDICT. *J. Atmos. Sci.* **69**: 1284−1305, doi: 10.1175/JAS-D-11-0225.1.

Dunkerton TJ, Montgomery MT, Wang Z. 2009. Tropical cyclogenesis in a tropical wave critical layer: Easterly waves. *Atmos. Chem. Phys.* **9**: 5587−5646, doi: 10.5194/acp-9-5587-2009.

Farazmand M, Haller G. 2012. Computing Lagrangian coherent structures from their variational theory. *Chaos (Woodbury)* **22**: 013128, doi: 10.1063/1.3690153.

Haller G. 2000. Finding finite-time invariant manifolds in two-dimensional velocity fields. *Chaos* **10**: 99−108, doi: 10.1063/1.166479.

Haller G. 2005. An objective definition of a vortex. *J. Fluid Mech.* **525**: 1−26, doi: 10.1017/S0022112004002526.

Haller G. 2011. A variational theory of hyperbolic Lagrangian coherent structures. *Physica D* **240**: 574−598, doi: 10.1016/j.physd.2010.11.010.

Haller G. 2015. Lagrangian cogerent structures. *Annu. Rev. Fluid Mech.* **47**: 137−162.

Haller G, Beron-Vera F. 2012. Geodesic theory of transport barriers in two-dimensional flows. *Annu. Rev. Fluid Mech.* **241**: 1680−1702.

Haller G, Beron-Vera F. 2013. Coherent Lagrangian vortices: The black holes of turbulence. *J. Fluid Mech.* **731**: 1−10, doi: 10.1017/jfm.2013.391.

Haller G, Poje A. 1997. Eddy growth and mixing in mesoscale oceanographic flows. *Nonlinear Processes Geophys.* **4**: 223−235, doi: 10.5194/npg-4-223-1997.

Hua BL, Klein P. 1998. An exact criterion for the stirring properties of nearly two-dimensional turbulence. *Physica D* **113**: 98−110, doi: 10.1016/S0167-2789(97)00143-7.

Ide K, Small D, Wiggins S. 2002. Distinguished hyperbolic trajectories in time-dependent fluid flows: Analytical and computational approach for velocity fields defined as data sets. *Nonlinear Processes Geophys.* **9**: 237−263, doi: 10.5194/npg-9-237-2002.

Jin DZ, Dubin DHE. 2000. Characteristics of two-dimensional turbulence that self-organizes into vortex crystals. *Phys. Rev. Lett.* **84**: 1443−1446, doi: 10.1103/PhysRevLett.84.1443.

Klein P, Hua BL, Lapeyre G. 2000. Alignment of tracer gradient vectors in 2D turbulence. *Physica D* **146**: 246−260, doi: 10.1016/S0167-2789(00)00119-6.

Lapeyre G, Klein P, Hua BL. 1999. Does the tracer gradient vector align with the strain eigenvectors in 2D turbulence? *Phys. Fluids* **11**: 3729−3737, doi: 10.1063/1.870234.

Lukovich J, Shepherd T. 2005. Stirring and mixing in two-dimensional divergent flow. *J. Atmos. Sci.* **62**: 3933−3954.

Lussier L, Rutherford B, Montgomery M, Dunkerton T, Boothe M. 2015. Examining the roles of the easterly wave critical layer and vorticity accretion during the tropical cyclogenesis of hurricane *Sandy*. *Mon. Weather Rev.* **143**: 1703−1722.

Mancho A, Wiggins S, Curbelo J, Mendoza C. 2013. Lagrangian descriptors: A method for revealing phase space structures of general time-dependent dynamical systems. *Commun. Nonlinear Sci. Numer. Simul.* **18**: 3530−3557, doi: 10.1016/j.cnsns.2013.05.002.

Montgomery M, Nicholls M, Saunders A, Cram T. 2006. A vortical hot tower route to tropical cyclogenesis. *J. Atmos. Sci.* **63**: 355−386.

Montgomery MT, Wang Z, Dunkerton TJ. 2010. Coarse, intermediate and high resolution numerical simulations of the transition of a tropical wave critical layer to a tropical storm. *Atmos. Chem. Phys.* **10**: 10803−10827, doi: 10.5194/acp-10-10803-2010.

Okubo A. 1970. Horizontal dispersion of floatable trajectories in the vicinity of velocity singularities such as convergences. *Deep Sea Res.* **17**: 445−454.

Pérez-Muñuzuri V, Huhn F. 2013. Path-integrated Lagrangian measures from the velocity gradient tensor. *Nonlinear Processes Geophys.* **20**: 987−991, doi: 10.5194/npg-20-987-2013.

Riemer M, Montgomery M. 2011. Simple kinematic models for the environmental interaction of tropical cyclones in vertical wind shear. *Atmos. Chem. Phys.* **11**: 9395−9414.

Rodrigue S, Eschenazi E. 2010. Lobe transport analysis of the Kelvin-Stuart cat's eyes driven flow. *Chaos* **20**: 013101, doi: 10.1063/1.3272714.

Rom-Kedar V, Leonard A, Wiggins S. 1990. An analytical study of transport, mixing and chaos in an unsteady vortical flow. *J. Fluid Mech.* **214**: 347−394.

Roulstone I, White AA, Clough SA. 2015. Geometric invariants of the horizontal velocity gradient tensor and their dynamics in shallow-water flow. *Q. J. R. Meteorol. Soc.* **140**: 2527−2534.

Rutherford B, Dangelmayr G. 2012. Lagrangian coherent structures in tropical cyclone intensification. *Atmos. Chem. Phys.* **12**: 5483−5507, doi: 10.5194/acp-12-5483-2012.

Rutherford B, Montgomery M. 2012. A Lagrangian analysis of a developing and non-developing disturbance observed during the PREDICT experiment. *Atmos. Chem. Phys.* **12**: 11355−11381, doi: 10.5194/acp-12-1-2012.

Shadden SC, Katija K, Rosenfeld M, Marsden JE, Dabiri JO. 2007. Transport and stirring induced by vortex formation. *J. Fluid Mech.* **593**: 315−331, doi: 10.1017/S0022112007008865.

Smith RK, Montgomery MT. 2012. Observations of the convective environment in developing and non-developing tropical disturbances. *Q. J. R. Meteorol. Soc.* **138**: 1721−1739, doi: 10.1002/qj.1910.

Tory K, Kepert J, Sippel J, Nguyen C. 2012. On the use of potential vorticity tendency equations for diagnosing atmospheric dynamics in numerical models. *J. Atmos. Sci.* **69**: 942−960, doi: 10.1175/JAS-D-10-05005.1.